Title
THE EFFECT OF SCHMIDT NUMBER ON THE FARADAIC IMPEDANCE

Authors
Hauser, A.K.
Newman, J.

Publication Date
1988-08-01

LBL-25721
Preprint

Lawrence Berkeley Laboratory
UNIVERSITY OF CALIFORNIA

Materials & Chemical Sciences Division

Submitted to Journal of the Electrochemical Society

The Effect of Schmidt Number on the Faradaic Impedance

A.K. Hauser and J. Newman

August 1988

Prepared for the U.S. Department of Energy under Contract Number DE-AC03-76SF00098.

DISCLAIMER

LBL-25721

The Effect of Schmidt Number on the Faradaic Impedance

Alan K. Hauser and John Newman

Materials and Chemical Sciences Division
Lawrence Berkeley Laboratory

and

Department of Chemical Engineering
University of California
Berkeley, CA 94720

August 21, 1988

LBL-25721

The Effect of Schmidt Number on the Faradaic Impedance

Alan K. Hauser and John Newman

Materials and Chemical Sciences Division, Lawrence Berkeley Laboratory,
and Department of Chemical Engineering, University of California,
Berkeley, CA 94720

August 21, 1988

Abstract

Frequency-response results, as calculated by the Stefan-Maxwell macroscopic impedance model, are presented for a copper rotating disk in chloride solutions. The working algorithm uses concentrated-solution theory and accounts for multicomponent diffusion, migration, and homogeneous and heterogeneous reactions, as well as a finite Schmidt number and interfacial velocity. The validity of the general program was checked by comparing the concentrated-solution model in the limit of dilute solutions, excess of supporting electrolyte, and infinite Schmidt number to known analytic solutions. Excellent agreement was obtained. Results for copper dissolution are plotted in various forms, enabling additional information about the given electrochemical system to be obtained. Specifically, the effect of the Schmidt number on the frequency-response of the faradaic impedance has been examined. Finally, a new way of plotting the dimensionless convective-diffusion impedance is proposed to reduce the Schmidt number dependence of the frequency response nearly to one curve by stretching the abscissa using $(\omega/\Omega)Sc^{1/3}$.

---

key words: Stefan-Maxwell multicomponent transport, rotating disk, copper dissolution

1. Introduction

A macroscopic impedance model,[1] requiring a numerical solution, has been presented. The objective of this paper is to use the developed algorithm to calculate the frequency response of a rotating-disk electrode. The working model utilizes the Stefan-Maxwell multicomponent transport equations to describe diffusion and migration in concentrated solutions with chemical and electrochemical reactions. Although the general model is capable of predicting the impedance behavior of many systems, only results for the anodic dissolution of copper in chloride solutions are presented.

The electrodissolution of a copper rotating disk has been studied experimentally using an ac-impedance technique[2] and has been found to be largely mass-transfer controlled, but a kinetic contribution could be identified at high rotation rates. For low current densities and Cl^- concentrations less than about 1 M, copper dissolves anodically in acidic chloride solution to form $CuCl_2^-$ in the following overall reaction

$$Cu + 2Cl^- \rightarrow CuCl_2^- + e^- \quad . \tag{1}$$

2. Method

The Stefan-Maxwell model is used to predict the frequency dependence of the faradaic and dimensionless mass-transfer impedance functions as a function of Schmidt number. The faradaic impedance, $Z_F = \tilde{V}/\tilde{i}_f$, is calculated by linearizing the copper dissolution kinetic expression

$$i_f = F k_a' c_{Cl^-,0}^2 \exp\left(\frac{(1-\beta)F}{RT} V\right) - F k_c' c_{CuCl_2^-,0} \exp\left(-\frac{\beta F}{RT} V\right) \tag{2}$$

using a Taylor expansion around the steady-state values of $\bar{c}_{i,0}$ and $\bar{V}$

$$\tilde{i}_f = \left(\frac{\partial i_f}{\partial V}\right)_{c_i}\Bigg|_{\bar{c}_{i,0},\bar{V}} \tilde{V} + \sum_i \left(\frac{\partial i_f}{\partial c_i}\right)_V\Bigg|_{\bar{c}_{i,0},\bar{V}} \tilde{c}_{i,0} \quad . \tag{3}$$

The electric driving force V used in the modified Butler-Volmer equation 2 is defined to be the electrode potential relative to a reference electrode of a given kind placed just outside the diffuse part of the double layer.

The alternating-faradaic-current-density equation 3 can be rearranged yielding the faradaic impedance for a single electrode reaction

$$Z_F = R_t - R_t \sum_i \left(\frac{\partial i_f}{\partial c_i}\right) \frac{\tilde{c}_{i,0}}{\tilde{i}_f} \quad , \tag{4}$$

where the charge-transfer resistance is given by $R_t = (\partial i_f/\partial V)^{-1}$. Thus, the faradaic impedance includes not only the effect of the faradaic charge-transfer reaction but also that of any concentration variations at the electrode surface that affect the rate of the electrochemical reaction.

The dimensionless mass-transfer impedance function is defined as the ratio of the alternating concentration to its derivative

$$\left\{ \frac{-1}{\theta_i'(0)} \right\} = \frac{\tilde{c}_{i,0}}{\tilde{c}'_{i,0}} \quad , \tag{5}$$

where $\tilde{c}_{i,0}$ and $\tilde{c}'_{i,0}$ are calculated using the Stefan-Maxwell model. The prime denotes differentiation with respect to the dimensionless distance $\xi = z\,(\Omega/\nu)^{1/2}\,(a\nu/3D_R)^{1/3}$, where ξ properly scales the rotating-disk problem[3] and D_R is the diffusion coefficient of the $CuCl_2^-$ reference species.

A goal of this paper is to check the validity of the generalized concentrated-solution-theory program by comparing the model results for certain limiting conditions (low concentrations and high, but finite Sc) to the dimensionless, convective-Warburg

impedance. The frequency dependence of the convective-Warburg impedance is characterized by the dimensionless quantity[4] $-1/\theta'(0)$, where θ is the solution to the frequency-dependent, convective-diffusion equation valid for infinite Schmidt number and dilute solutions with no migration.[5]

Smyrl[2] previously used an approach similar to the method just discussed to study the mixed kinetic- and mass-transfer-controlled copper-chloride system. The $-1/\theta'(0)$ function was combined with a kinetic expression similar to equation 2, and with equation 3, a resulting equation for the faradaic impedance enabled both the diffusion coefficient and the kinetic rate constants to be determined from impedance data using a limited frequency range. Recently, Morris and Smyrl[6] have used a numerical fitting procedure to analyze the entire frequency spectrum for the ferricyanide-ferrocyanide redox system.

We should like to continue such an analysis by investigating the effects of mass transfer on the faradaic impedance by arbitrarily varying the Schmidt number, while the solution composition, the electrode potential, and the rotation rate are kept constant. The Stefan-Maxwell results, for a wide frequency range, will be plotted in various forms, enabling kinetic and mass-transfer information pertaining to a given electrochemical system to be obtained. The analysis is applicable to redox systems, as well as to the mixed kinetic and mass-transfer controlled copper dissolution process to be discussed in this paper.

Before presenting the results, let us discuss the model input parameters. The rate constants used in equation 2 for the copper dissolution process are the same as in references [7] and [8] for the case of an infinite homogeneous rate constant ($\hat{k}_b = \infty$) and

are summarized in table 1.† The steady-state potential relative to a saturated calomel reference electrode is $\overline{V} = -0.205$ V, and unless specified otherwise, all reported results are for a copper disk rotating at 2000 rpm in 0.1 N HCl with a kinetic viscosity of $\nu = 8.9 \times 10^{-3}$ cm^2/s at $T = 298.15$ K. For this system, the copper chloride complex (reference species), $CuCl_2^-$, has a Schmidt number of 1567.

3. Faradaic Impedance

The computer-generated results of the Stefan-Maxwell model for the dissolution of a copper rotating disk are plotted in figure 1 on the complex plane. This Nyquist plot shows the negative of the imaginary part of the faradaic impedance, $-Z_F$, *versus* the real part of Z_F (with the frequency as a parameter) for a Schmidt number of 1567. No

Table 1. Model input parameters for the dissolution of copper in 0.1 N HCl.

$k_a' = 10^3$ cm^4/mol·s	$k_c' = 10^{-1}$ cm/s
$D_{H^+} = 9.31 \times 10^{-5}$ cm^2/s	$D_{Cl^-} = 2.03 \times 10^{-5}$ cm^2/s
$D_{CuCl_2^-} = 0.568 \times 10^{-5}$ cm^2/s	(base case)
$D_{CuCl_2^-} = \nu/Sc$ where	$Sc = 10^x$ and $x = 2,3,4$

† In another paper,[9] we develop a generalized procedure for obtaining the fundamental and necessary input parameters from experimental impedance data. The data reduction scheme is based on analytic equations for the faradaic impedance.

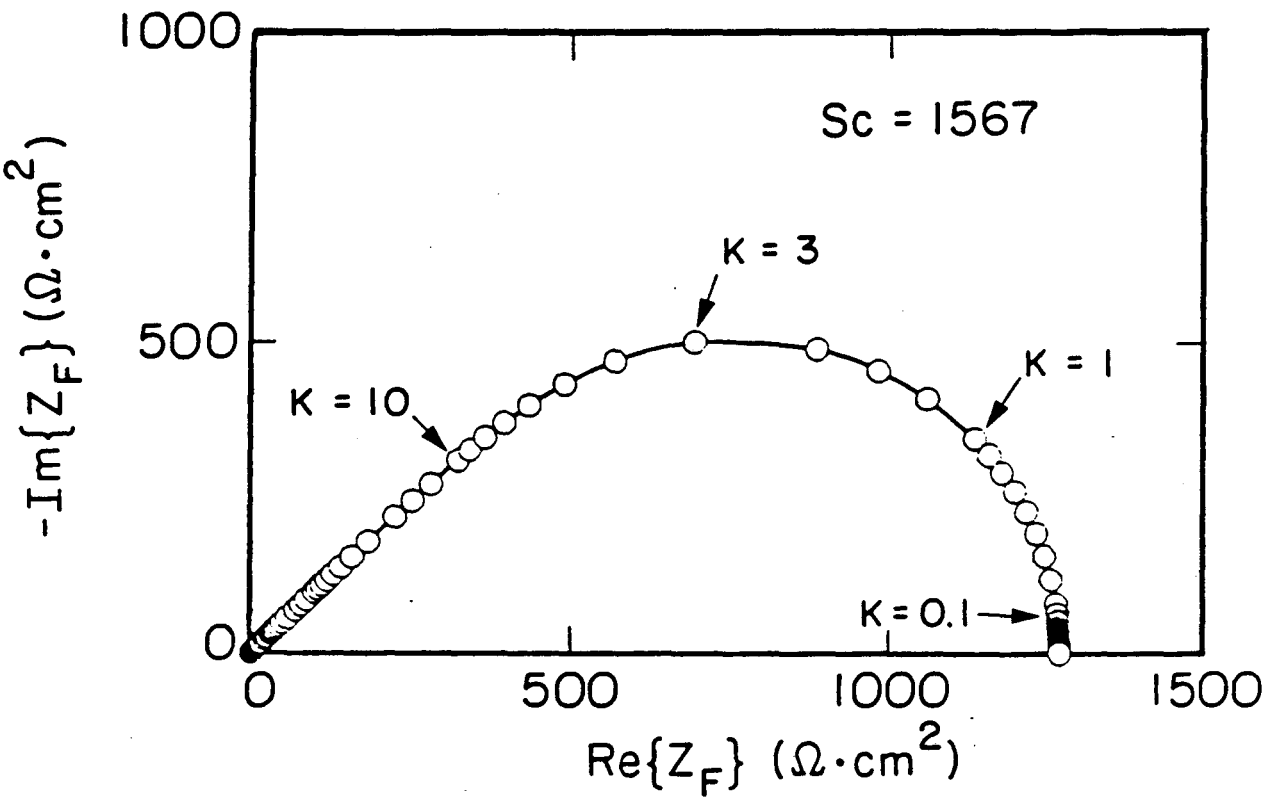

Figure 1. Nyquist plot of the faradaic impedance for the anodic dissolution of copper.

double-layer charging effects or electrolyte resistance are included in this figure. Therefore, a capacitive semicircle does not appear to the left of the mass-transfer loop. The dimensionless frequency $K = \omega\nu(3D_R/a\nu)^{2/3}/\Omega D_R$ is a parameter for the plot with eleven points per decade (1, 1.3, 1.6, 2, 3, 4,$\cdots$9).

Plotting the results in this form enables the effect of each component of the faradaic impedance, $Z_F = R_t + Z_0$, to be studied. The charge-transfer resistance, $R_t = \lim_{\omega\to\infty} \{Z_F\}$, is the high-frequency limit of the faradaic impedance and is a kinetic parameter independent of mass-transfer. For the fast electrode kinetics of the copper system, R_t is so small (1.44 $\Omega\cdot cm^2$), as would be expected for a Nernst-like (reversible) reaction, that it is negligible in figure 1. Z_0 is the mass-transfer impedance resulting from concentration variations at the surface due to convection and diffusion and is the remaining effect of the faradaic impedance after R_t is subtracted.

The charge-transfer resistance is obtained at the high-frequency limit because the time scale is so short that diffusion cannot influence the current. Since the surface concentration does not change significantly from the mean value, the diffusion impedance drops out at high frequency, and charge-transfer kinetics alone dictate the current.

As we move away from the high-frequency limit, along the curve toward the right, (as the frequency decreases) we observe a linear relation between Re $\{ Z_F \}$ and Im $\{ Z_F \}$ characterizing a diffusion-controlled electrode process. An infinite Nernst diffusion-layer thickness leads to a straight line with a slope of unity, known as the classical Warburg impedance. However, accounting for convection at the rotating disk yields finite values for both the diffusion-layer thickness and the convective-Warburg

impedance at the low-frequency limit and this gives rise to the loop shown in figure 1.

In the low-frequency range, the frequency dependence of the diffusion impedance changes. Instead of both the real and imaginary parts of the impedance being proportional to $1/\sqrt{\omega}$ (as at high frequencies), the imaginary part is proportional to the frequency, whereas the real part is proportional to the square of the frequency. This change is due to the effect convection has on the process.

An important quantity to be derived from such measurements is the impedance at zero frequency, where the imaginary part goes to zero and the real part is finite and is shown on the right of the figure. This low-frequency limit represents the steady-state polarization resistance $R_p = \lim_{\omega \to 0} \{Z_F\}$. R_p is the sum of the charge-transfer resistance R_t and $R_0 = \lim_{\omega \to 0} \{Z_0\}$, the steady-state limit of the mass-transfer impedance Z_0.

Figure 2 is a Nyquist plot of the faradaic impedance as function of Schmidt number. For purposes of comparison, Schmidt numbers of 100, 1000, and 10,000 are shown in addition to the base case of $Sc = 1567$. Its effect on the polarization resistance is significant, while the charge-transfer resistance is independent of Sc. All four curves for different Schmidt numbers in figure 2 are shown to be converging to a value of $R_t = 1.44\ \Omega \cdot \mathrm{cm}^2$ in the limit of high frequency. The large effect of the Schmidt number on R_p may be explained by the relationship the polarization resistance has with the resistance to mass transfer. For example, for the largest $Sc = 10{,}000$ shown in figure 2, R_p is the largest, implying the greatest resistance to mass transfer or small mass-transfer rates. As Sc decreases, the diffusion coefficient increases (assuming constant viscosity), yielding smaller and smaller resistance to mass transfer. Thus, as $Sc \to 0$, or

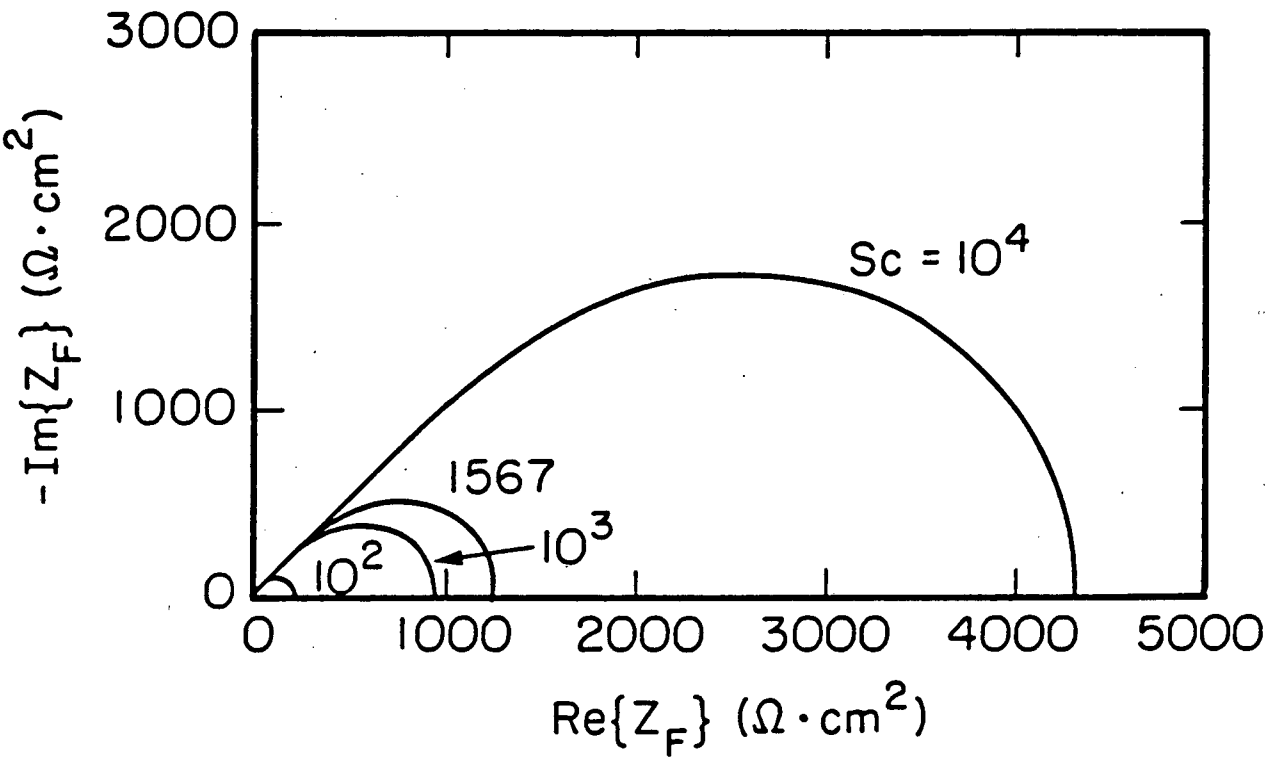

Figure 2. Nyquist plot of faradaic impedance as a function of *Sc*.

$D_i \rightarrow \infty$, there would be no diffusion impedance, and the convective-diffusion loop would disappear completely, implying rapid mass transfer. Similar effects could be obtained by varying the angular rotation speed of the disk, Ω. An infinite rotation rate would yield the same result as $Sc \rightarrow 0$.

The polarization resistance R_p is an important quantity in impedance studies since it can be shown to be related to the steady-state current density and thus, the dissolution rate of the metal. The results given in figure 2 can be used to shed more light on understanding the present dissolution problem. To do this, the real part of the faradaic impedance is plotted versus $-p\ \mathrm{Im}\{Z_F\}$ in figure 3, where $p = \omega/\Omega$ is a dimensionless perturbation frequency. K is related to p by $K = 3.2576 p Sc^{1/3}$. The entire frequency range is shown in this figure, with the important low-frequency limit at the left.

Smyrl[2],[10] first demonstrated that this way of plotting the data (a Smyrl plot) allows the real part of the impedance to be extrapolated to zero frequency easily, because a straight line can be fitted to the low-frequency data in figure 3, and the imaginary part should be zero at zero frequency.

The three different Schmidt-number curves in figure 3, as for figure 2, converge in the limit of high frequency to a value of $R_t = 1.44\ \Omega{\cdot}\mathrm{cm}^2$. The $Sc = 100$ case approaches the limit the fastest because, at a given frequency, the low Sc minimizes mass-transfer effects.

The low-frequency limit of the impedance is important because we are interested in examining the convective-diffusion impedance Z_0. Therefore, the previous plot is shown again in figure 4, where only the low-frequency region is shown. Over a limited

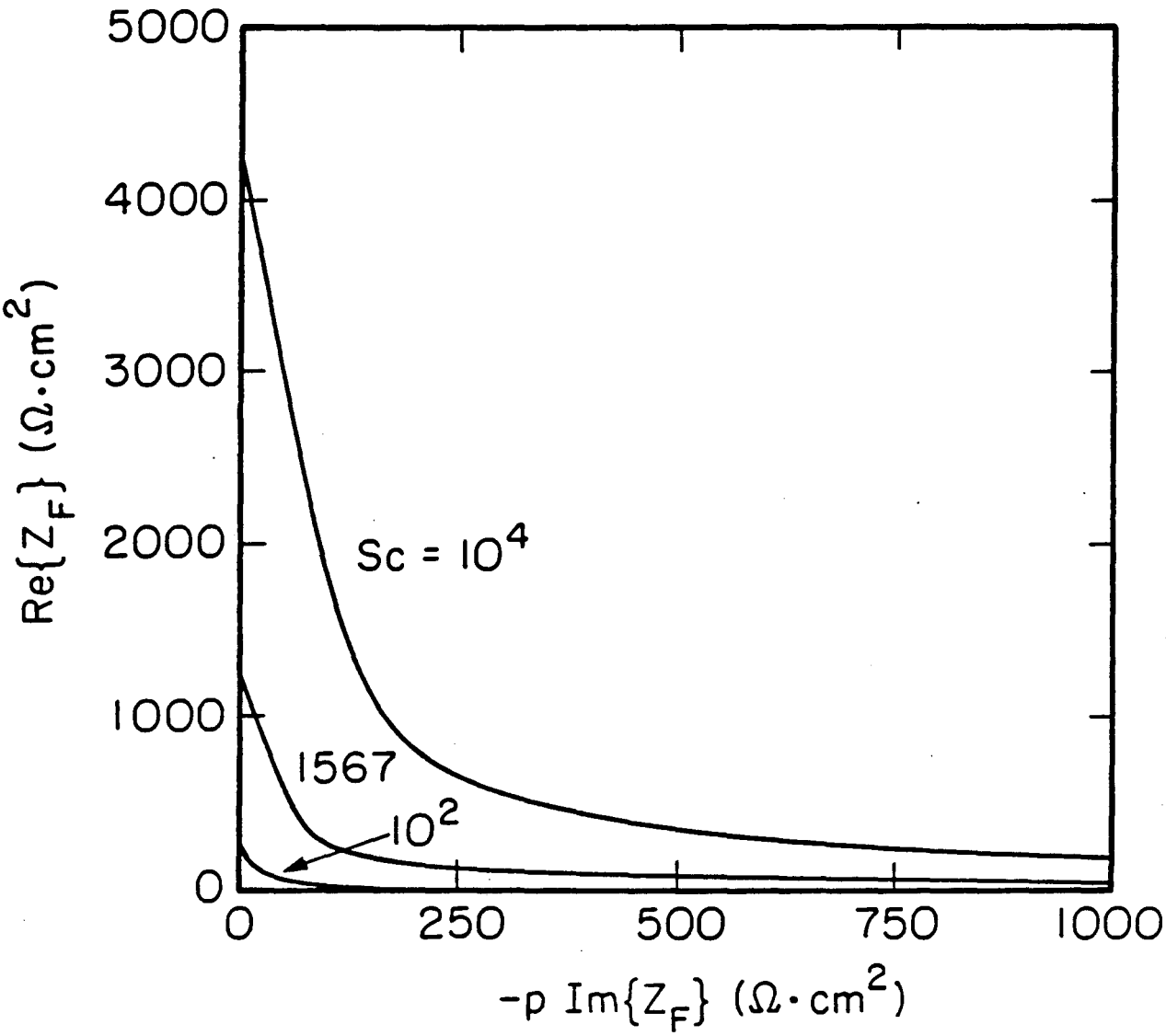

Figure 3. Smyrl plot of the faradaic impedance as a function of *Sc*.

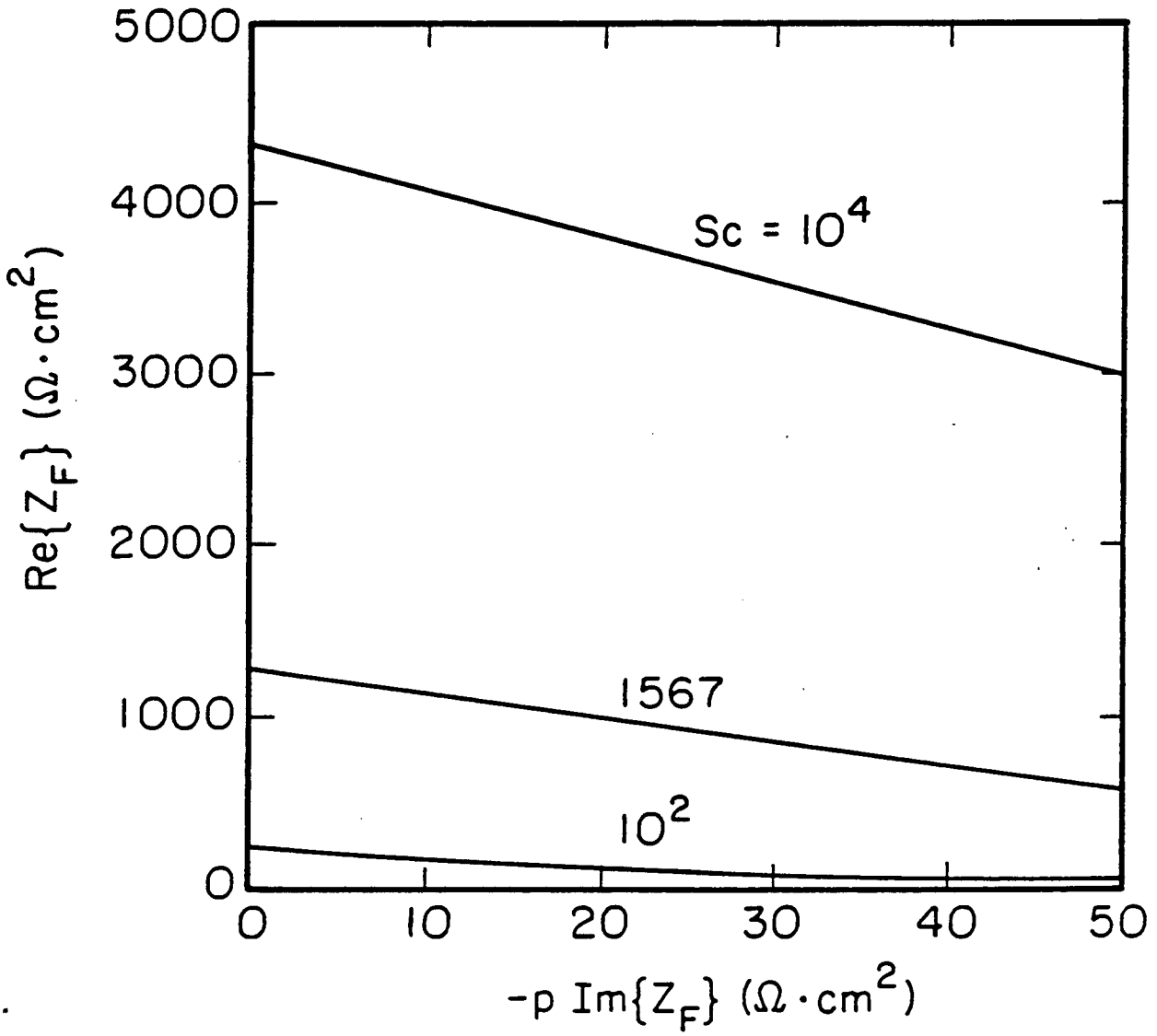

Figure 4. Smyrl plot of the low-frequency region of the faradaic impedance.

frequency range, the frequency response is linear.

It is interesting to examine the magnitude of the slopes as a function of Schmidt number. The real part of the faradaic impedance increases with Sc, and the magnitude of the slope is proportional to $Sc^{1/3}$. Thus, the slope can be used to extract the diffusion coefficient of the system being investigated.[2] Also, this procedure is a good check of the model results. Finally, the program enables one to investigate whether the Smyrl plot allows the Schmidt number to be determined correctly from figure 4 when kinetics is involved. This latter effect has yet to be quantified.

4. Dimensionless, Mass-Transfer Impedance

The frequency dependence of the dimensionless mass-transfer impedance $-1/\theta_i'(0)$, given by equation 5, is shown on the complex plane in figure 5. The real and imaginary parts of the impedance for the three Schmidt numbers, 100, 1567, and 10,000, are given. The frequency at a curve maximum is the characteristic frequency ($K = 3$) and yields the mass-transfer time constant.

An advantage of plotting the frequency dependence of the $-1/\theta_i'(0)$ impedance function is that the infinite Schmidt number case, the dilute-solution convective-Warburg impedance $-1/\theta'(0)$, can be shown. When the exact solution to the frequency-dependent convective-diffusion equation at infinite Schmidt number is compared to the Stefan-Maxwell model results for the dimensionless convective-diffusion impedance, generally good agreement is found, with the larger Schmidt-number results yielding obviously the best agreement. However, the effect of Sc on the low-frequency $-1/\theta_i'(0)$ impedance function is shown in figure 5 to be the opposite of the Sc effect on the

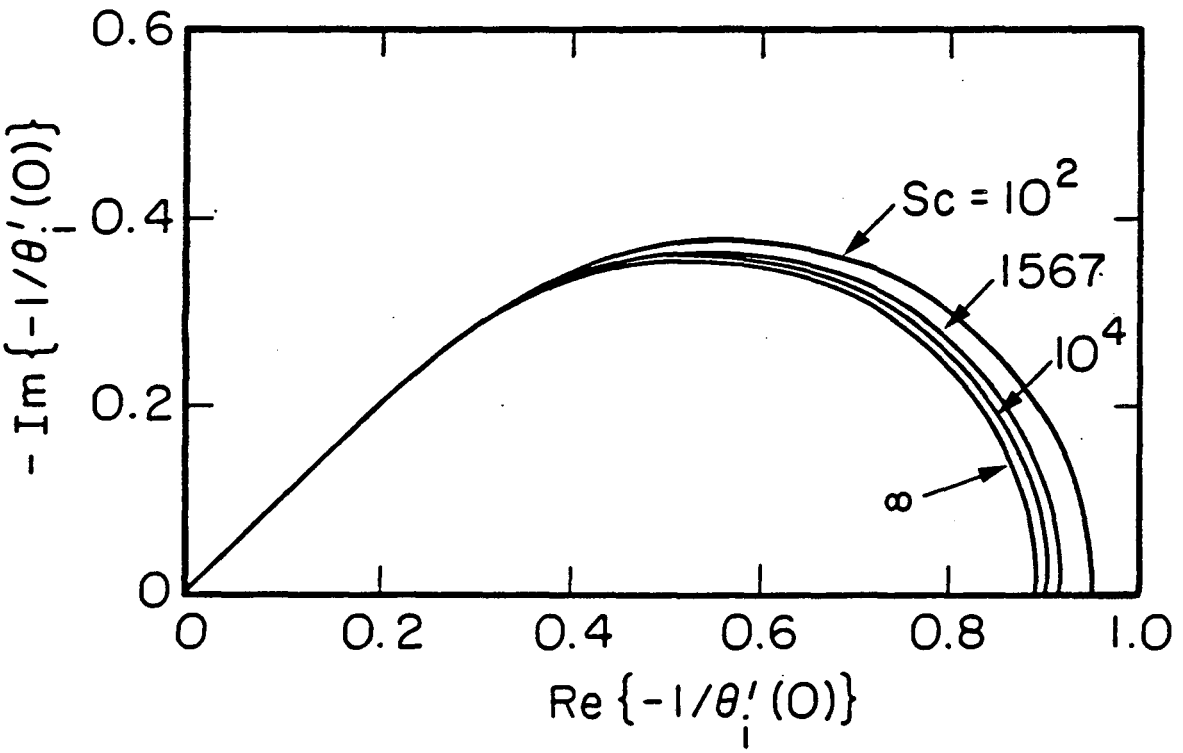

Figure 5. Nyquist plot of the dimensionless convective-diffusion impedance.

faradaic impedance that was given in figure 2. The low-frequency limits of the finite-Schmidt-number calculation of the dimensionless impedance function are slightly greater than that for infinite Sc, and these results will be discussed in the next section.

The results at the low frequencies may be further explained by plotting the real part of $-1/\theta_i'(0)$ *versus* p times the negative of the imaginary part of $-1/\theta_i'(0)$ as shown in figure 6. This allows us to examine the Schmidt number dependence of the dimensionless convective-diffusion impedance function $-1/\theta_i'(0)$ in the same way that the faradaic impedance was plotted in figure 4. Plotting the data in this fashion allows the dimensionless steady-state resistance due to convective diffusion $R_d = \lim_{\omega \to 0} \{-1/\theta_i'(0)\}$ to be determined as a function of Schmidt number. R_d can then be related to the steady-state dimensionless mass-transfer rate, which will provide a check of the validity of the Stefan-Maxwell model. These results, calculated using Newman's[11] steady-state mass-transfer rates to a rotating disk for Sc of 100 and 10,000, are hardly visible on the intercept of the ordinate. These steady-state results could be plotted *versus* $Sc^{-1/3}$; however, this has not been done. Instead, the calculations will be presented in tabular form and will be discussed in the next section.

Lastly, a plot of Re $\{-1/\theta_i'(0)\}$ *versus* $-pSc^{1/3}$Im $\{-1/\theta_i'(0)\}$, as shown in figure 7, reduces the Schmidt number dependence of the curves. Interestingly, plotting the data in this form over the entire frequency range yields just one curve, any deviations are in the low-frequency range and are shown in more detail in figure 6. This latter effect can be explained by the thicker boundary layer at lower frequencies. Hence, the convective effect, or Sc correction, is most significant at steady state, where the multiple term velocity series is needed.

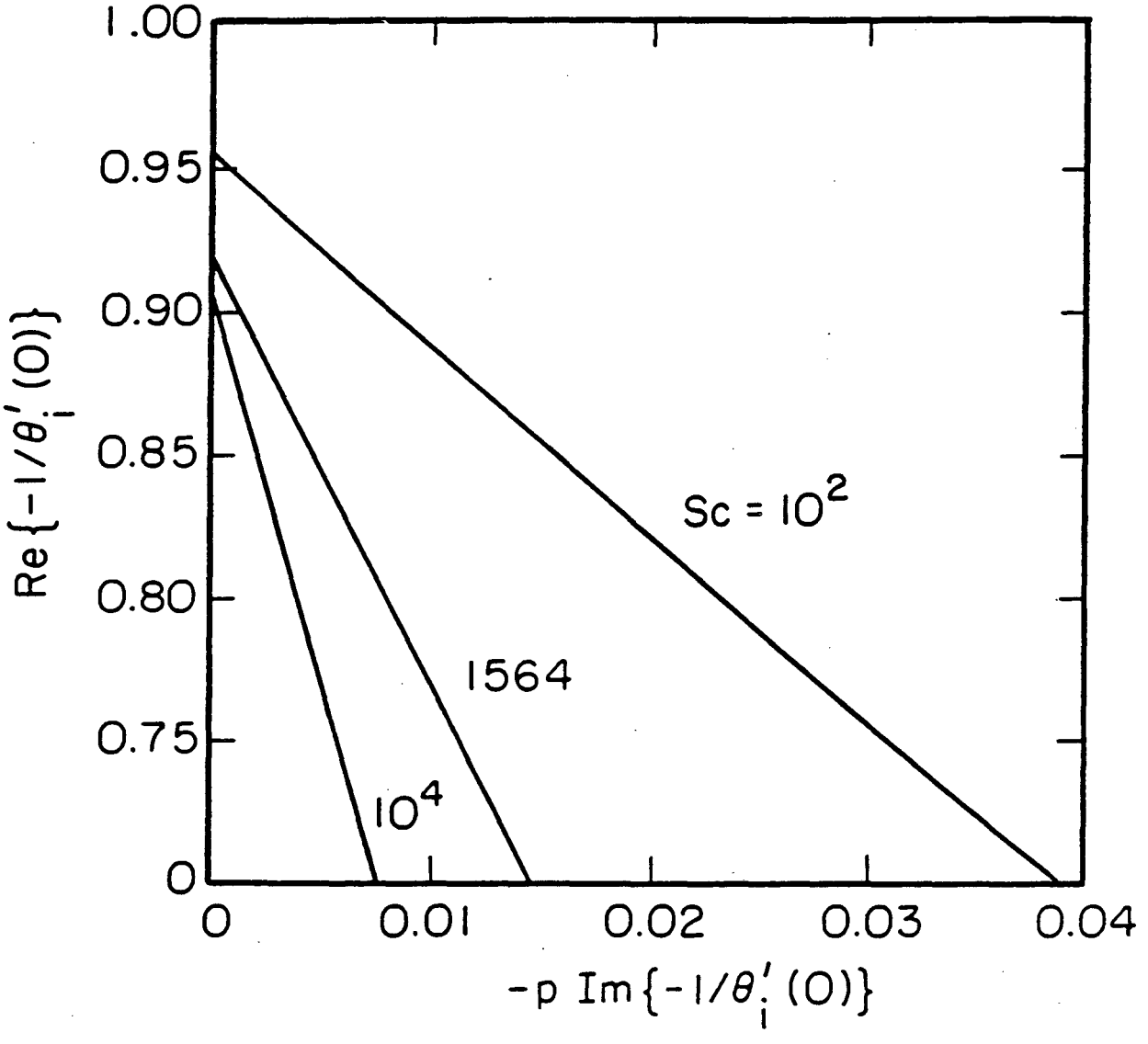

Figure 6. Smyrl plot of the dimensionless, convective-diffusion impedance for several values of *Sc*.

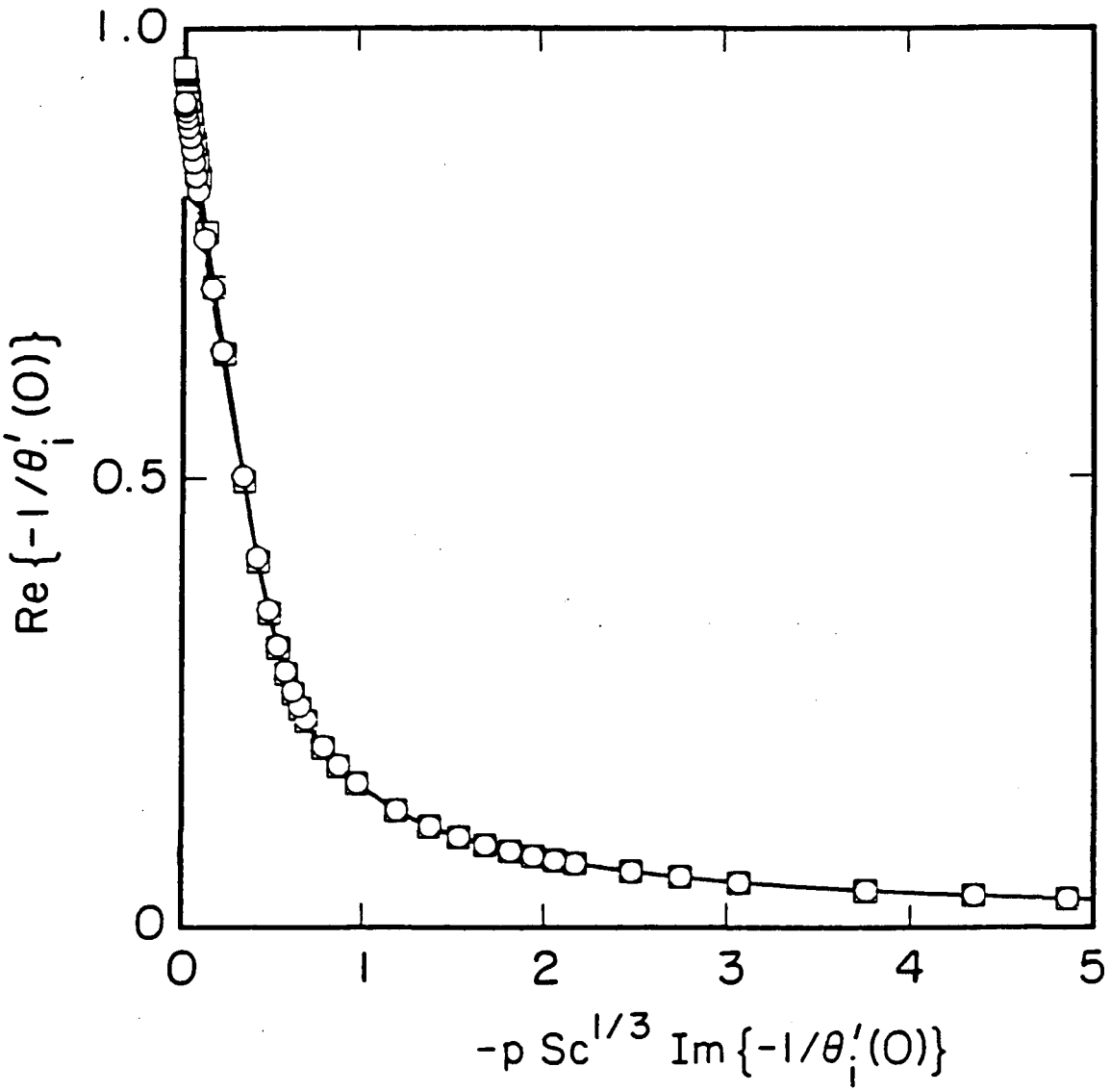

Figure 7. Plot of the dimensionless convective-diffusion impedance as a function of *Sc* covering a larger frequency range than figure 6 and with the abscissa stretched with the value of the Schmidt number.

5. Discussion of Results

First, let us discuss the validity of the numerical model. For purposes of comparing the Stefan-Maxwell-program results to the dilute-solution, convective-Warburg-impedance results,[4,5] the case of low electrolyte concentration (0.1 N HCl) and a low anodic overpotential ($\overline{V} = -0.205$ V) has been investigated, similar to reference [12]. This is the simplest case to model accurately and to predict the current density; dilute-solution theory may be used since there are no strong interactions among species which require concentrated-solution theory. Also, the low potential means little dissolution of copper will occur, resulting in the copper chloride species concentration being very small compared to the electrolyte. This implies that the effect of migration will be small due to small amount of $CuCl_2^-$ relative to the supporting electrolyte.

The original goal of comparing the low-frequency limits of the Stefan-Maxwell impedance results to previous steady-state, mass-transfer work can be done by using the following relationship

$$\lim_{\omega \to 0} \left\{ \frac{-1}{\theta_i'(0)} \right\} = \left(\frac{a\nu}{3D_i} \right)^{1/3} \frac{1}{\Theta_i'(0)} = A \frac{Sc^{1/3}}{\Theta_i'(0)} = A \left(\frac{Sc}{\Theta_i'(0)} \right) Sc^{-2/3} . \tag{6}$$

The low-frequency limit of the dimensionless impedance function $-1/\theta_i'(0)$ is related to the dimensionless steady-state mass-transfer rate to a rotating disk, $\Theta_i'(0)/Sc$, where Θ_i is defined as $\Theta_i = (c_i - c_{i,0})/(c_{i,\infty} - c_{i,0})$ and $A = 0.55405$. The prime used in the mass-transfer rate denotes differentiation with respect to $\varsigma = z(\Omega/\nu)^{1/2}$ as opposed to ξ, which is used in the dimensionless impedance function.

Values of the steady-state limit of the dimensionless impedance, calculated using concentrated-solution theory as a function of Sc, can be compared to the mass-transfer

resistance $A\ Sc^{1/3}/\Theta_i'(0)$, calculated using the steady-state, dilute-solution mass-transfer rates, accounting for the Sc correction,[11] but with no migrational effects. These comparisons were illustrated graphically in figure 6 for $p = 0$ (the ordinate values on the Smyrl plot of the dimensionless impedance function) and are given in table 2. Excellent agreement between the Stefan-Maxwell-model results and the steady-state, dilute-solution rates of mass-transfer is seen. The small differences can be attributed to either the effect of migration, the interaction of species in solution with each other, or in part to finite-differences error. The Sc-correction effect at low frequency results in a difference of up to 7% between Schmidt numbers of 100 and infinity.[11] This yields the maximum error due to Sc differences, since the dc result is most sensitive to the Schmidt number correction. For the ac case at higher frequencies, the Sc correction is

Table 2. Comparison of the Stefan-Maxwell model's low-frequency limit of the dimensionless, mass-transfer impedance (161 and 321 mesh points) with the results using the steady-state dilute-solution mass-transfer rate.

Sc	$A\frac{Sc^{1/3}}{\Theta_i'(0)}$	$\lim_{\omega \to 0}\left\{\frac{-1}{\theta_i'(0)}\right\}$		Error (%)	
		mesh points		mesh points	
		(161)	(321)	(161)	(321)
100	0.95694	0.95625	0.95625	−0.07	−0.07
1000	0.92096	0.92206	0.92211	0.12	0.12
1567	0.91717	0.91802	0.91809	0.09	0.10
10,000	0.90529	0.90645	0.90681	0.13	0.17
∞	0.89298	0.89404	0.89411	0.12	0.13

less important because the diffusion boundary layer is smaller due to the short time frame. Hence, the extra terms in the velocity profile become less important.

Let us now discuss the different Schmidt-number dependence of the impedance that was illustrated in the previous figures. For example on figure 6, $\Gamma(4/3)$ is the lower limit on the ordinate axis. The correction for finite Sc increases the real part of the dc limit of $-1/\theta_i'(0)$. Thus, the low-frequency limit of the dimensionless convective diffusion impedance increases slightly with decreasing Sc. In figure 4, just the opposite behavior is found; the low-frequency limit of the faradaic impedance, R_p, or of the dimensional diffusion impedance, R_0, increases with Sc. This behavior should be compared to the Sc dependence of the mass-transfer rate.

Levich[13] showed that the large-Schmidt-number asymptote for the mass-transfer rate Θ_i'/Sc is proportional to $Sc^{-2/3}$. In other words, the mass-transfer rate decreases with increasing Schmidt number, since a large Sc implies a small diffusion coefficient, and thus small mass-transfer rates. Therefore, the faradaic impedance results shown in figures 2, 3, and 4 can be justified physically since an impedance or resistance to mass transfer should decrease with decreasing Sc.

6. Conclusions

The Stefan-Maxwell macroscopic-transport model has been used to calculate the faradaic impedance as a function of frequency for the anodic electrodissolution of a copper rotating disk in hydrochloric acid solutions.

First, the validity of the developed program was checked by comparing the concentrated-solution model to analytic solutions in the limit of dilute solutions and

infinite Schmidt number. The need for such checks cannot be overemphasized when using and developing complex computer programs of this nature. Excellent agreement was obtained for the copper system, confirming the validity of the model.

Secondly, the mathematical model was used to study the effect of the Schmidt number on the frequency response of the mass-transfer controlled process. A new way of plotting the dimensionless convective-diffusion impedance was proposed that reduces the Schmidt number dependence of the frequency response nearly to one curve by stretching the abscissa using $(\omega/\Omega)Sc^{1/3}$. Finally, a theoretical study of the electrochemical impedance method is extremely important because it allows one to discover new ways of analyzing impedance measurements.

Acknowledgements

This work was supported by the Assistant Secretary for Conservation and Renewable Energy, Office of Energy Storage and Distribution of the U.S. Department of Energy under Contract DE—AC03—76SF00098.

List of Symbols

a	0.51023
A	$(a/3)^{1/3} = 0.55405$
$c_{i,0}$	concentration of species i at the electrode surface, mol/cm^3
$\overline{c}_i$	steady-state concentration of species i, mol/cm^3
D_i	dilute-solution diffusion coefficient of species i, cm^2/s
e^-	symbol for the electron
f	frequency, Hz
F	Faraday's constant, 96,487 C/equiv
$\overline{i}$	steady-state current density, A/cm^2
i_f	faradaic current density, A/cm^2
$\tilde{i}_f$	alternating faradaic current density, A/cm^2
k_a', k_c'	anodic and cathodic rate constant for a charge-transfer reaction
$\hat{k}_b$	backward rate constant for the homogeneous reaction,
K	dimensionless frequency
p	ω/Ω, dimensionless frequency
R	universal gas constant, 8.3143 J/mol-K
R_t	electron-transfer resistance, ohm·cm^2
R_p	polarization resistance, ohm·cm^2

R_0	low-frequency limit of the mass-transfer impedance Z_0, ohm·cm^2
R_d	low-frequency limit of the dimensionless, mass-transfer impedance
Sc	Schmidt number
T	absolute temperature, K
$\tilde{V}$	alternating kinetic driving force (electrode potential relative to given reference electrode placed just outside double layer), V
$\bar{V}$	steady-state part of kinetic potential driving force, V
Z_F	complex faradaic impedance, ohm-cm^2
Z_0	complex mass-transfer part of faradaic impedance, ohm-cm^2
Z_W	complex convective-Warburg impedance, ohm-cm^2

Greek symbols:

β	symmetry factor
$\Gamma(4/3)$	0.89298, the gamma function of 4/3
$-1/\theta_i'(0)$	complex, dimensionless, mass-transfer impedance function for species i
$-1/\theta'(0)$	complex, dimensionless, convective-Warburg impedance function for species i
Θ_i	dimensionless concentration of species i
$\frac{\Theta_i'(0)}{Sc}$	dimensionless steady-state mass-transfer rate of species i
ν	kinematic viscosity, cm^2/s

ω	perturbation frequency, rad/s
Ω	angular rotation speed of disk, rad/s

subscripts:

a	anodic
b	back reaction
c	cathodic
0	just outside the diffuse part of the double layer
∞	in the bulk electrolyte, where there are no concentration variations

superscripts:

$-$	time-average or steady-state part
$\sim$	complex, time-independent part

References

[1]. Alan K. Hauser and John Newman, "A Macroscopic-Impedance Model for a Rotating-Disk Electrode. I. Theoretical Treatment of the Electrochemical Impedance Using Concentrated-Solution Theory," to be submitted to *Journal of the Electrochemical Society* (1988).

[2]. William H. Smyrl, "Digital Impedance for Faradaic Analysis. II. Electrodissolution of Cu in HCl," *Journal of the Electrochemical Society, 132,* 1555-1562 (1984).

[3]. John Newman, *Electrochemical Systems,* Englewood Cliffs, N. J.: Prentice-Hall, Inc., 1973.

[4]. Robert V. Homsy and John Newman, "An Asymptotic Solution for the Warburg Impedance of a Rotating Disk Electrode," *Journal of the Electrochemical Society, 121,* 521-523 (1974).

[5]. E. Levart and D. Schuhmann, "Comparison of Some Solutions for the Warburg Impedance of a Rotating Disk Electrode," *Journal of the Electrochemical Society, 122,* 1082-1083 (1975).

[6]. Rael Morris and William Symrl, "Digital Impedance for Faradaic Analysis. IV. Rigorous Treatment of Rotating Disk Electrode Impedance Over the Entire Frequency Range," to be submitted to *Journal of the Electrochemical Society* (1988).

[7]. Alan K. Hauser and John Newman, "Effects of Finite Rates of a Homogeneous Reaction on the Dissolution of Copper in Chloride Solutions," submitted to *Journal of the Electrochemical Society.*

[8]. Alan K. Hauser and John Newman, "Singular Perturbation Analysis of the Faradaic Impedance of Copper Dissolution Accounting for the Effects of Finite Rates of a Homogeneous Reaction," submitted to *Journal of the Electrochemical Society.*

[9]. Alan K. Hauser and John Newman, "A Macroscopic-Impedance Model for a Rotating-Disk Electrode. II. Analytical Forms of the Impedance for Data Reduction," to be submitted to *Journal of the Electrochemical Society* (1988).

[10]. Bernard Tribollet, John Newman, and William H. Smyrl, "Determination of the Diffusion Coefficient from Impedance Data in the Low-Frequency Range," *Journal of the Electrochemical Society, 135,* 134-138 (1988).

[11]. John Newman, "Schmidt Number Correction for the Rotating Disk," *Journal of Physical Chemistry, 70,* 1327-1328 (1966).

[12]. Bernard Tribollet and John Newman, "Impedance Model for a Concentrated Solution. Application to the Electrodissolution of Copper Solutions," *Journal of the Electrochemical Society, 131,* 2780-2785 (1984).

[13]. Veniamin G. Levich, *Physical Hydrodynamics,* Englewood Cliffs, N. J.: Prentice-Hall, Inc., 1962.

LAWRENCE BERKELEY LABORATORY
TECHNICAL INFORMATION DEPARTMENT
UNIVERSITY OF CALIFORNIA
BERKELEY, CALIFORNIA 94720